

WEATHER RADAR NETWORK WITH PULSE COMPRESSION OF ARBITRARY NONLINEAR WAVEFORMS: KA-BAND TEST-BED AND INITIAL OBSERVATIONS

H. Lee and Y.-H. Kim

School of Information and Mechatronics
Gwangju Institute of Science and Technology
261 Cheomdan-gwagiro, Buk-gu, Gwangju 500-712, Republic of Korea

Abstract—Short-wavelength radar networks are expected to complement current long-range weather radar systems. Accordingly, we proposed a configuration for such a network constituting pulse compression radars in order to use frequency resources efficiently and obtain multi-static information. We developed high resolution Ka-band pulse compression weather radar system as a test-bed. Using a commercial direct digital synthesizer (DDS) and field programmable gate array (FPGA) control, we generated linear and arbitrary nonlinear frequency modulated waveforms for low range sidelobes. Further, we completed a high duty factor system with a solid-state power amplifier. In a vertical-pointing mode, we were able to employ the developed radar to detect moderate rainfall up to 15 km. Details of the system design, hardware structure, data acquisition and processing algorithms were described. To validate the performance of the proposed radar system, we conducted several experiments by measuring cloud, snow and rain.

1. INTRODUCTION

Recently, abnormal weather events, such as short-time, localized torrential rains, have occurred more frequently on the Korean Peninsula. Due to such events, accurate sensing and analysis of meteorological phenomena has become even more critical. From a wide array of meteorological sensors, weather radar plays a significant role in such phenomena, especially for short-term weather prediction and hazardous weather alerts. The most commonly

used parameters within weather radar are reflectivity and velocity, derived from electromagnetic wave energy backscattered by the precipitation particles and Doppler information along the radar beam axis. In addition, the introduction of polarization schemes has enabled researchers to distinguish various precipitation particles for better estimation and prediction.

Current operational weather radars are most commonly represented by S- or C-band high power pulse radars using tube-based devices such as magnetrons or klystrons. Corresponding detection usually ranges over hundreds of kilometers. For such radars, to obtain reasonable spatial resolution at long distances, the diameter of antenna aperture should be lengthy, although greatly increasing system size and cost. In particular, due to the Earth's curvature, the lower part of the troposphere is not easily detectable by means of long-range radars. Moreover, such radars are not effective for network extension in surroundings with much terrain blockage. Of note, about 70 percent of Korea includes such a obstruction via dense mountain. High power devices affect system stability, safety and price.

Researchers have attempted to supplement or substitute such long-range radar networks with distributed dense networks using small short-wavelength radar systems via leading groups such as CASA [1] and NIED [2]. Using X-band test-beds with magnetron-based radars, such systems have discernibly enhanced adaptive scanning and collaborative sensing.

Meanwhile, various researchers have tried to use pulse compression technique in weather radar [3–7]. It transmits long modulated pulses and compresses corresponding echo signals, resulting in finer range resolution with the lower peak power. For a given resolution, as opposed to pulse radar, it is estimated to provide increased sensitivity, possibility of the lower measurement error and higher scan speeds [4].

Although scarcely being considered in tandem previously, we based the present research on two such streams. Particularly, the main objective of this paper was to present not only an application based on pulse compression technology for a weather radar network, but also effective configuration. For validation, we developed a test-bed of high duty factor pulse compression radar with solid-state power amplifier in the Ka-band, arbitrary linear and nonlinear modulated waveforms being generated using fast FPGA control. We fully described the consideration of pulse compression techniques, linear and nonlinear digital waveform generation, detailed test-bed design and implementation, as well as initial experimental results, in the remaining sections.

2. WEATHER RADAR NETWORK

A small-clustered radar network, rather than one with single large-coverage radar, has advantages in terms of information quality and measurement reliability. By covering similar area with multiple radars, additional capabilities — such as dual-Doppler estimation of horizontal wind vectors or pinpoint tracking of storms — are provided. Also, the effective design of such network radar systems can provide reduced power and less antenna size.

Much research exists regarding the use of meteorological radar networks for sensing weather phenomenon [8–12]. Such work has focused on the node and network structures, data link and transmission, adaptive scanning and radar control as well as the advantages of small radar networks. Especially, CASA IP1 has implemented real enhanced network using four relatively low-powered X-band magnetron-based radars, the merits of each being clearly discernible.

Conversely, additional consideration regarding radar networks is required. In particular, the use of numerous narrow-pulse network radars is not efficient with regards to frequency resources and interference. Although a peak power, of tens of kilowatts, is relatively smaller than current large-scale operating radars, such radars still affect long distance areas and interfere with other radars or radio systems with common frequency bands. A multitude of frequency resources are eventually necessary for such network extensions, but they are finite. For example, although a range of 9.3 ~ 9.5 GHz is allotted for radar application in X-band — including the meteorological remote sensing — many military-purposed and marine radars have already used considerable available resources in such frequency band.

In regards to frequency resource, pulse compression radar systems can provide advantages in weather networks. For given resolution requirement, transmitting peak power is greatly reduced by employing relatively long pulses. Since radar detection ability depends on average rather other than peak power, peak power decreases with the use of high duty factor radar. Thus, the effects from neighboring transmitting power become less in pulse compression radar systems and this means frequency reuse planning, similar in cellular communication, is more applicable for small clustered radar networks. Moreover, because of low correlation between existing pulse radar waveforms and pulse compression radar, mutual interference — although dependent on design — is very slight.

Many materials exist for system extension about network design [13,14]. For optimal configuration of multi-radar networks

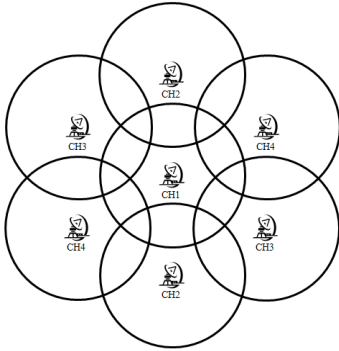


Figure 1. A hexagonal weather radar network using 4 different channels.

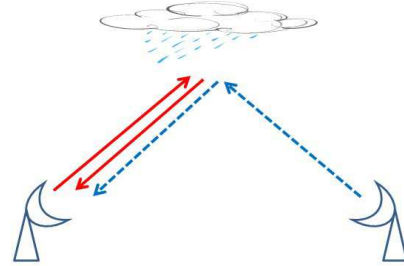


Figure 2. Simultaneous observation of mono- and bi-static signals.

especially regarding maximum dual-Doppler overlapping, hexagonal cell arrangement, i.e., joining three neighboring radar forms at a 60 degree angle, is most effective [15]. Fig. 1 depicts four channel usage (frequency bands) for such a configuration. Frequency reuse patterns are extendable with more numbers of channels translating into longer distances for identical channel sites.

Additionally, assuming scanning information for adjacent radar sites is available, radar possibly acquires bi- or multi-static data as shown in Fig. 2. Hence, dual or multi-Doppler estimation at a single site is possible. When original velocity vectors of the targets are similar to the direction of tangential beam injection, bi-static data is more effective in obtaining Doppler information. Although such results increase the data quality, mono- and bi-static signals should be processed simultaneously. Hence, we introduced identical baseband waveform for adjacent radars.

Figure 3(a) illustrates one example of X-band frequency allotment. If 15 MHz of bandwidth are used for very fine range resolution of 10 m, then nearly 12 channels will be available at X-band. By combining four channels into one band, then three bands become available. Such a band concept especially applies to frequency availability in a particular region. Radar system structures can be constructed as shown in Fig. 3(b). By the combination of LO1 frequencies (local oscillator 1) for band selection and LO2 (local oscillator 2) for channel selection, the desired channel signals are transmitted. In the receiver, the band is already selected by sharing LO1 with the transmitter and the channel is selected in the digital domain with IF under-sampling techniques. In fact, not only mono- but bi-static information from adjacent channel

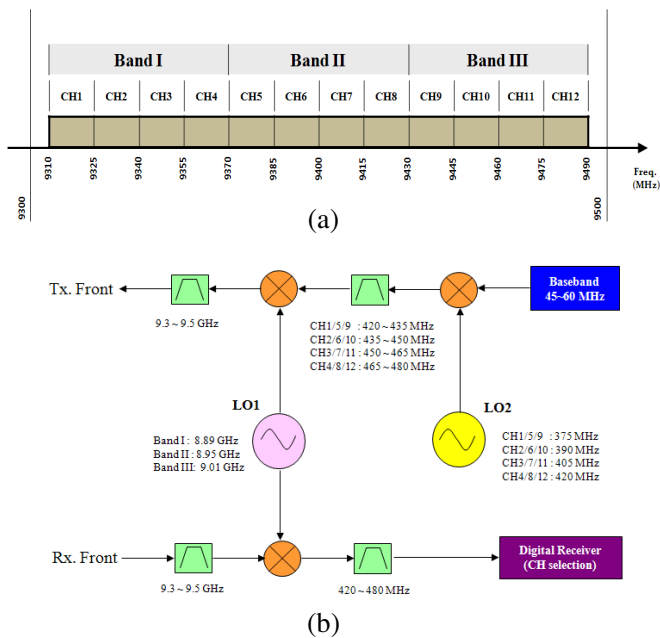


Figure 3. Radar network example in X-band: (a) Channel allotment. (b) Radar system structure.

signals can simply be extracted by adequately changing frequency values during down-converting signal processing. Such a concept has been experimentally verified with signal generation, acquisition and channel selection in signal processing easily.

3. ARBITRARY WAVEFORM GENERATION FOR PULSE COMPRESSION

The choice of pulse compression techniques depends primarily on waveform and processing. The frequency modulation makes the carrier frequency of the transmit waveform swept in a time domain. It is known to yield good range sidelobe performance comparing other methods [3]. Pulse compression has not been widely employed in weather radar primarily due to unignorable range sidelobes. Thus, in our test-bed, we selected pulse compression with frequency modulation rather than phase modulation.

To reduce the range sidelobes, pulse shaping in time and/or frequency domains should be applied. In time domain, since such

performance is affected by linearity of RF components, practical application was rendered difficult in high power circuits. In the case of a 128 μsec pulse and 10 MHz of modulation bandwidth, we applied several kinds of well-known window functions to the frequency domain. Accordingly, a mixture of Hamming and Blackman-Harris windows performed best within several combinations [16]. We generated linear frequency modulated waveform and demodulated using these window functions. Experimentally achievable peak sidelobe levels are nearly 50 \sim 60 dB.

Although several studies have relied on the previous schemes, disadvantages in power efficiency persist due to the filtering out a considerable quantity of power during window application. In avoiding such drawbacks, an additional approach includes direct generation of nonlinear waveform on transmitters. Although researchers analyze nonlinear waveform itself to reduce range sidelobes in weather radar application such as [17, 18], practical implementation is rare, especially in wideband areas [19]. We implemented nonlinear frequency modulated waveform using a commercially available DDS chip controlled by a FPGA programmed for high speed operation. Accordingly, as much as 50 MHz of chirp bandwidth was attainable, enabling high compression gains and opportunities for solid-state device usage.

Any kind of the window or nonlinear function can be used for waveform within the digital domain. We implemented such functions, as shown in Fig. 4, by initially selecting the desired frequency response of the determined nonlinear function in sufficient finite modulation bandwidth steps. Secondly, we integrated the function, achieving normalization. Thirdly, we calculated the inverse function and obtained the differential value directly related to DDS delta frequency, leading to regular interval change in frequency value.

In our experiments, the Blackmanharris window function was

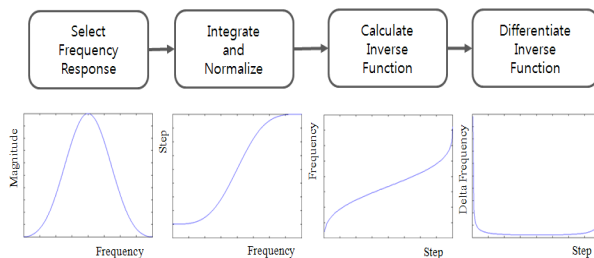


Figure 4. Nonlinear waveform generation steps.

used for nonlinear waveform generation. For 10 MHz of modulation bandwidth and 128 μ sec of pulsewidth, 160 steps — taking the reference clock rate into consideration — were selected for DDS control. From an equation of such a window function, the frequency response was obtained and accumulated in discrete time. The inverse function was acquired with a numerical method, final delta frequency data being used for FPGA control.

4. KA-BAND RADAR SYSTEM DESIGN

Although X-band radar has recently been hailed as an effective candidate for gap-filling or mobile operation within weather radar networks, we selected the Ka- instead of the X-band for system compactness in our feasibility study. Millimeter wavelength(MMW) radars, usually implemented at Ka- or W-band complement centimeter-wavelength radars due to the possession of more sensitive characteristics. Conversely, such radars are disadvantaged as a result of high attenuation. Several examples of research areas in MMW weather radar are the general cloud physics associated with climate-affecting cloud-radiation interaction, the weather modification activities, etc. [20, 21]. In Ka-band, 35.2 ~ 36 GHz of frequency band was allotted for meteorological aids service with other applications such as radiolocation service. We applied 12.5 MHz of bandwidth to one channel — including the some guard bands — as well as four channels in one band and with a total of 10 bands being available between 35.5 GHz and 36 GHz.

Table 1 shows major characteristics of the designed radar system [22].

In single antenna radar systems, a 128 μ sec pulse generates severely the problematic so-called blind zone in which only a partial eclipse of the signal's echo is encountered, due to the receiver being off during pulse transmission [23]. Although several previous researchers have detected this region by the presence of extra short pulses, degradation of system performance as well as system complexity, still persists [6, 24]. In our test-bed, we used dual antennas for the transmitter and the receiver in order to detect targets near the radar. For antennas, we used previously developed lens antennas with two degrees of beamwidth [25]. Further, we set Ka-band power at 5 W for the commercially available solid-state amplifier. As an initial step, we directed radar points vertically forward possibly useful for precipitation and cloud microphysical observation possessing a range up to 15 km. In addition, other parameters were primarily reconfigured via digital control.

Table 1. Major characteristic of the designed radar system.

Frequency	35.5 ~ 36 GHz
Chirp bandwidth	10 MHz ~ 12.5 MHz
Pulse width	128 μ sec
PRF	4 kHz
Power (Peak)	5 W
Noise figure	3 dB
Ant. gain	36 dBi
3 dB beamwidth	2.2°
Polarization	Linear (H)
A/D sampling rate	50 MHz
A/D resolution	14 bits
Observation range	10 ~ 15 km
Number of integration (N)	64

The system design was analyzed through a radar equation. A generally well-known meteorological radar equation, one form in the received power point is as follows:

$$P_r = \frac{P_T G_0^2 \Theta \Phi c \tau \pi^3 |K|^2 Z}{512(2 \ln 2) \lambda^2 r^2} \quad (1)$$

In the case of pulse compression, pulses were much longer than ones in general pulse radars, which is related to compression gain. Such length actually enhanced minimum detectable value of radar reflectivity. For analysis of noise power, compression filter bandwidth should be applied. Minimum detectable reflectivity of pulse compression radar Z_{0l} is

$$Z_{0l} = Z_0 \frac{\tau B_c}{\tau_l B} \quad (2)$$

where Z_0 and B represents the minimum detectable reflectivity and general pulse radar bandwidth and B_c is compression filter bandwidth. For identical bandwidth, nearly 30 dB enhanced sensitivity was expected in the present case. By applying the proposed system design parameter, without consideration of additional attenuation, radar was expected to detect approximately -25 dBZ of reflectivity for targets at 1 km, -5 dBZ at 10 km and 0 dBZ at 15 km, including 64 non-coherent integrations.

5. DESIGN OF TRANCEIVER

Figure 5 shows an overall block diagram of the current developing system. This system was composed of a waveform generator, a transmitter, two antennas, a receiver, a synthesizer, a data acquisition unit and a computer for signal processing of pulse compression and data processing of weather parameter extraction.

Using a 300 Msamples/s quadrature DDS chip (Analog Device, AD9854) and FPGA (Altera cyclone EP1C69240C8) control, various frequency modulated signals were generated below 60 MHz of bandwidth by means of premade files in a table format based on a waveform generation method. For a 128 μ sec pulse, 160 steps were used for sweeping frequency with a 200 MHz clock made from a 10 MHz external reference. For 100 MHz data acquisition rate, baseband chirp signals ranging from 38.75 ~ 48.75 MHz were made, being generally used throughout experimentation.

In the transmitter, the baseband FM signal was initially up-converted to IF, a 450 ~ 500 MHz region of the selected channel, by using a LO2 PLL synthesizer at 412.5/425/437.5/450 MHz. A single sideband mixer was used for quadrature inputs, and image rejection stood at more than 40 dB. After amplification and additional filtering, the signal was up-converted to the Ka-band using a LO1 PLL Synthesizer with a double balanced mixer. After RF waveguide bandpass filter, 5 W of commercially available SSPA (solid-state power amplifier) module (Quinstar) was applied. A variable attenuator was inserted for optimal power transmission. Before antenna port employment, an OMT (orthomode transducer) was utilized for future dual polarization vis-à-vis simultaneous transmitter and receiver schemes.

30cm-diameter lens and corrugated horns for feeders were

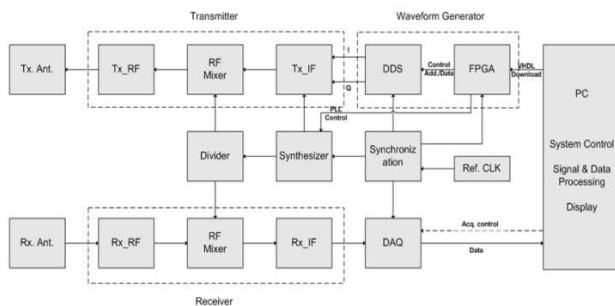


Figure 5. Block diagram of the test-bed radar.

developed and used for the antenna. In such a configuration, the lens likewise functioned as a radome, possessing plano-convex shape and made by means of dielectric polycarbonate material. Zoning was employed to reduce lens weight. A circular corrugated horn offered a nearly circularly symmetric radiation pattern, as well as reduced cross-polarization. During near field measurement and far-field analysis, a gain of 36 dBi and a 3 dB beamwidth of 2.2 degrees were revealed. Cross-polarization was approximately 35 dB in the absence of an OMT. During azimuth plane measurement, sidelobes levels were less than -30 dB.

At the receiver, an OMT was present for dual polarization after antenna deployment. A low noise amplifier (LNA) of 2.8 dB noise figure was used and the noise figure of the receiver path is below 4 dB including several passive components before LNA. Using the LO1, which is used simultaneously in the transmitter, the received RF signal was down-converted to a 450 ~ 500 MHz IF frequency and directly connected to the data acquisition unit with the level being adjusted according to additional amplifying and filtering stages stood at a maximum power of 10 dBm with 50Ω impedance.

The LO1 originated from the X-band PLL module (Z-comm PSA3007C) with a frequency multiplier; the LO2 was derived directly from the PLL module (Z-comm PSA0413). For the LO1, a power divider was utilized for both transmitter and receiver. For fully coherent processing, DDS, FPGA, the data acquisition unit and two PLL synthesizer modules were all synchronized with a common reference clock of 10 MHz. For network operation, a GPS clock was applicable for such a purpose.

The received IF signal was then transferred to the data acquisition unit with a triggering signal that revealed the starting point of the generated pulse. It is directly connected to the ADC. Using the analog filter before ADC deployment as well as under-sampling (bandpass sampling) technique, the signal was still able to be fully reconstructed during signal processing. Signal processing and data processing were built in MATLAB in the feasibility study. Our group currently continues such research by means of parallel FPGA and DSP implementation.

6. DESIGN OF PROCESSING

Digitized data were processed on the PC. Processing was divided into signal processing by extracting IQ data via pulse compression and data processing in order to extract the parameters, i.e., received power and velocity from IQ data.

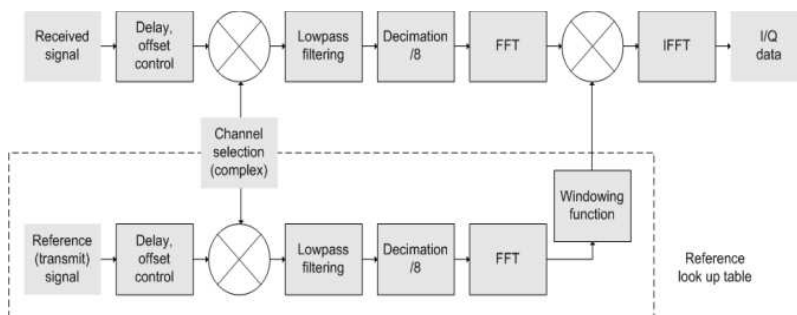


Figure 6. Signal processing flow diagram.

As shown in Fig. 6, the first stage of the processing involved the digital down converter block, translated 100 MHz digitized samples into complex data consisting of in-phase (I) and quadrature (Q) components. During radar network consideration, multi-static data from the adjacent sites were acquired by changing only channel selection frequency during down converting. If the signal processing block had been built parallel, the radar would have obtained bi- and mono-static data simultaneously. Low-pass anti-aliasing filter and output data-reducing decimator were deployed. In our case, the decimation number stood at eight, determined by the ratio of the chirp bandwidth and the sampling rate. For pulse compression, correlation processing was performed using FFT (Fast Fourier Transform) in the frequency domain. Complex conjugate values of the reference data, sampled from transmitted pulse and converted in the frequency domain were multiplied with receiving data. And this value was again converted to the time domain value using IFFT (inverse FFT). Before IFFT, weighting functions (windows) were used on the compressed pulse spectrum in order to reduce sidelobe levels. However, this also broadened mainlobe width and degraded range resolution slightly. Various window functions such as Hamming, Hanning, Blackman and Blackman-Harris, were applicable. For LFM (linear frequency modulation) waveform, the combination of Hamming and Blackman-Harris were applied. For the NLFM (nonlinear frequency modulation), waveform itself demonstrated window function characteristics with our proposed method, thus being more effective than LFM in point of power conservation.

Data processing was initiated by arraying complex discrete signals resulting during signal processing of pulse compression within the observation range. Fig. 7 reveals the block diagram of the present data processing scheme. By arraying $N = 64$ pulse repetition interval

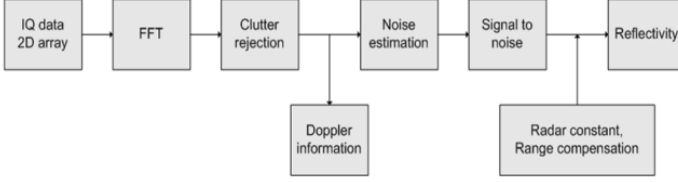


Figure 7. Data processing flow diagram.

samples and applying FFT, the discrete power spectrum of the signal was thus acquired. Afterwards, the S/N (signal to noise ratio) as well as Doppler velocity and spectrum width were estimated. Although more than 70 dB of cross coupling existed between transmitter and receiver due to antenna separation, a considerable amount of power nevertheless flowed directly into the receiver chain. For rejections of non-moving clutters as well as such cross coupling effects, a fixed-width clutter filter method was employed, removing zero-Doppler spectrum components and interpolating across the gap. To obtain the S/N from received signals, noise power was estimated by the mean power of reference noise heights where, as it is assumed, no meteorological targets existed. By establishing experimentally-determined threshold values related to noise variation, the scattered signal spectrum was thus obtained.

The meteorological radar reflectivity factor was measured in dBZ, as follows:

$$Z(\text{dBZ}) = 10 \log [Z (\text{mm}^6/\text{m}^3)] = 10 \log [10^{-18} \cdot Z (\text{m}^6/\text{m}^3)] \quad (3)$$

For convenience, the reference height H_0 was also introduced, as follows:

$$10 \log(SNR) = 10 \log \left[\frac{P_T G_0^2 \lambda^2 c \tau \Theta \Phi}{1024 \pi^2 \ln 2 \cdot L \cdot (k_B T_0 F_N B)} \cdot \frac{\pi^5 |K|^2}{\lambda^4} \cdot \frac{1}{H_0^2} \cdot 10^{-18} \right] + 10 \log \left(\frac{H^2}{H_0^2} \right) + Z(\text{dBZ}) \quad (4)$$

Introducing radar constant C (dB), we had the following:

$$C(\text{dB}) = -10 \log \left[\frac{P_T G_0^2 \lambda^2 c \tau \Theta \Phi}{1024 \pi^2 \ln 2 \cdot L \cdot (K_B T_0 F_N B)} \cdot \frac{\pi^5 |K|^2}{\lambda^4} \cdot \frac{1}{H_0^2} \cdot 10^{-18} \right] \quad (5)$$

$$Z(\text{dBZ}) = C(\text{dB}) + 20 \log \left(\frac{H}{H_0} \right) + SNR(\text{dB}) \quad (6)$$

7. INITIAL OBSERVATIONS

The test-bed radar was installed at the top of our department building on the campus of GIST, Gwanju, Korea in January of 2010. Accordingly, several experiments were conducted.

For the initial radar function verification, installation was executed by horizontally pointing radar at known ground targets such as buildings. In such a setup, radar was used with only 20 dBm output power. Fig. 8 shows the measurement of relative intensity based on

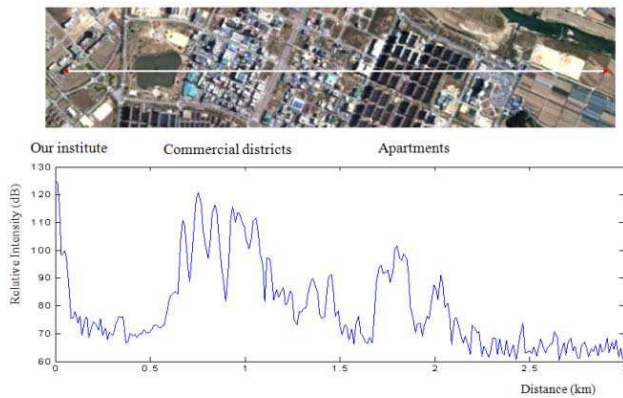


Figure 8. Ground target detection.

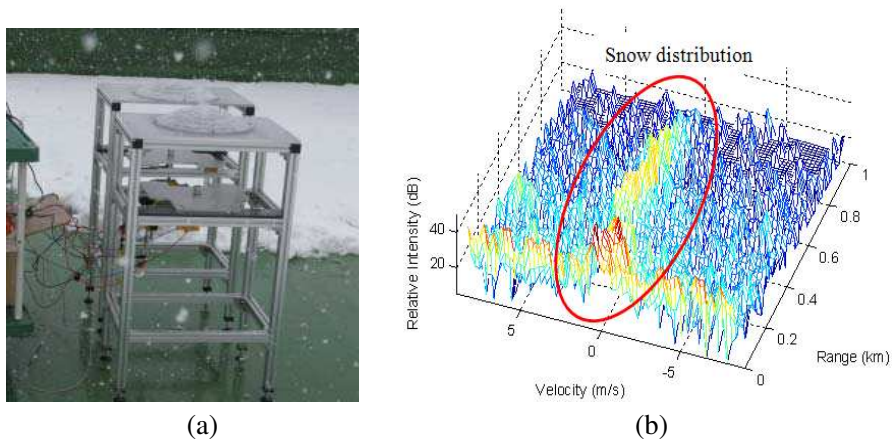


Figure 9. Snow detection: (a) A Photo of the designed radar with separated Tx. and Rx. antennas, (b) Doppler spectrum measured at 13:58 on January 13th 2010.

pulse compression. Up to about 0.5 km, there is only low altitude area and after that there are relative high reflectivity targets from commercial buildings and apartments. Measurements results agreed with map data qualitatively.

While the 13th of January, 2010, witnessed snow, the radar pointed in a vertical direction as shown in Fig. 9. Compared with other forms of precipitation, snow has the characteristics of relatively low refractive index and it demonstrates low reflection. Short wavelength radar is more advantageous in detecting snow. Despite being weak, we confirmed that radar was able to detect snow signals from as far away as 1 km. Because of the distance between antennas, low altitude observation area was smaller than observation with single antenna system. Based on frequency analysis, velocity components of snow were distributed at nearly zero.

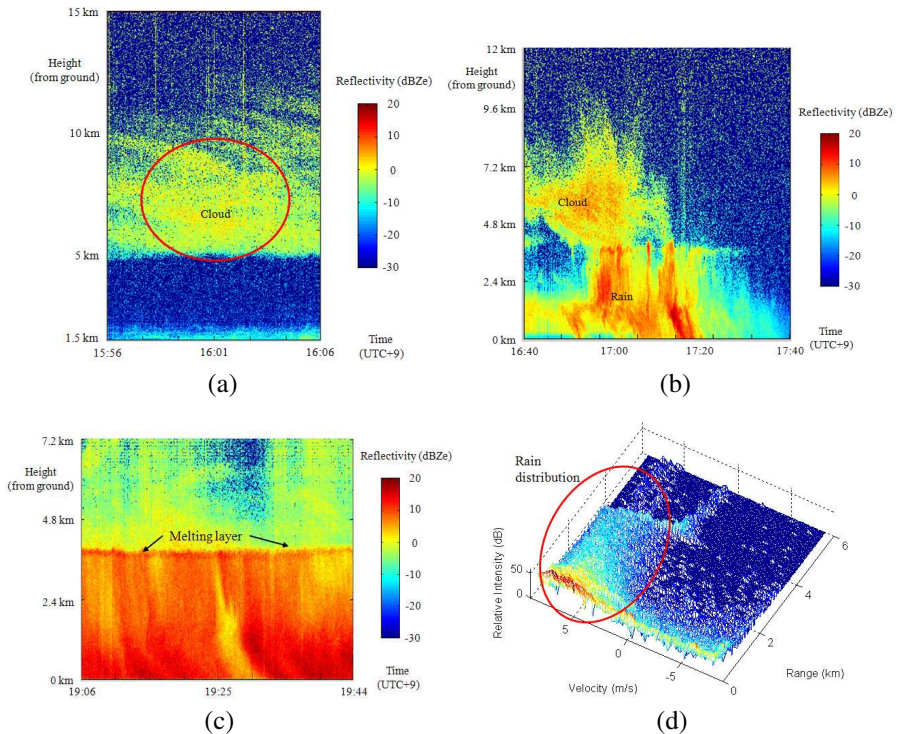


Figure 10. Observation on 17th of May 2010: (a) Detection of cloud (LFM, 2 sec resolution), (b) Detection of cloud and rain (NLFM, 5 sec resolution), (c) Detection of rain (NLFM, 2 sec resolution), (d) Doppler spectrum of rain measured at 19:10.

A middle rain event occurred on the 17th of May 2010. For measurement, we sequentially employed a 128- μ sec pulsewidth, 10 MHz bandwidth LFM and NLFM. Pulse repetition time stood at 250 μ sec, while recorded resolution was 2 and 5 seconds. For Doppler processing, 64 numbers of pulses were used. Examples of the time-height cross section of reflectivity are shown in Fig. 10(a) denotes the case of LFM and 2 seconds of time resolution. Radar was able to detect middle stratus clouds spread above 5 km. Further, (b) and (c) are cases of the NLFM and 5 seconds of time resolution. At (b), there was rain after 17:00. From such a figure, we observed changing stages ranging from moisture clouds to rain. At (c), during rain, we clearly observed the bright band (melting layer) which precipitation materials transformed into water at 3 km. Our radar had about 15 m of range resolution, being very suitable for researching such kinds of bright bands. One particular Doppler spectrum at an altitude between 0 ~ 5 km and measured at 19:10, is shown in (d). Just below the bright band at 4 km, reflectivity increased rapidly, while velocity also increased from 0 to 7 ~ 8 m/sec.

8. CONCLUSION

Short wavelength radar systems are expected to supplement current long-range radar network for low altitude troposphere observation. Such systems possess advantages with regards to compactness and improved sensitivity. Accordingly, we proposed a weather observation network composed of pulse compression radars for efficient frequency use and low interference. By sharing identical baseband waveform while varying intermediate frequency, such a radar system can easily obtain multi-static information from adjacent sites within digital domains.

In this paper, we presented pulse compression radar with arbitrary waveforms to validate the systematic concept of the proposed radar network. A frequency modulation method was implemented using DDS chip and FPGA control for radar waveform generation. By means of calculating delta frequencies in the digital domain, arbitrary kinds of linear or nonlinear waveforms were generated using the suggested method. Millimeter waves of 35 GHz were selected for the test-bed with 5 W SSPA being used for the power device. Using a radar equation, the system was estimated to detect approximately -5 dBZ at 10 km. We described the waveform generator, transmitter, antennas, receiver, synthesizer, data acquisition unit and processing algorithms for pulse compression and weather parameter extraction in detail.

We have been conducting initial tests in our institute since

January of 2010. In particular, 15 m of spatial resolution and 2 seconds of time resolution were attained near the ground. By pointing in a vertical direction, radar was able to detect clouds and snow, in which relatively low levels of reflectivity are difficult to detect with centimeter wavelength radar. During rainfall observation, we observed both cloud and rain, being able to confirm a bright band.

In future experimentation, radar will be verified by comparing observations with other sensors. Moreover, attenuation effects should also be investigated in more detail and reflected in algorithms. Finally, we plan to extend research to include dual polarization and scanning structures.

ACKNOWLEDGMENT

This work was supported in part by the Brain Korea program (BK21) at Gwanju Institute of Science and Technology, Korea and millisys, Inc. of Korea.

REFERENCES

1. McLaughlin, D., D. Pepyne, V. Chandrasekar, B. Philips, J. Kurose, M. Zink, K. Droegemeier, S. Cruz-Pol, F. Junyent, J. Brotzge, D. Westbrook, N. Bharadwaj, Y. Wang, E. Lyons, K. Hondl, Y. Liu, E. Knapp, M. Xue, A. Hopf, K. Kloesel, A. Defonzo, P. Kollias, K. Brewster, R. Contreras, B. Dolan, T. Djaferis, E. Insanic, S. Frasier, and F. Carr, "Short-wavelength technology and the potential for distributed networks of small radar systems," *Bulletin of the American Meteorological Society*, Vol. 90, 1797–1817, December 2009.
2. Maki, M., T. Maesaka, R. Misumi, K. Iwanami, S. Suzuki, A. Kato, S. Shimizu, K. Kieda, T. Yamada, H. Hirano, F. Kobayashi, A. Masuda, T. Moriya, Y. Suzuki, A. Takahori, D. Lee, D. Kim, V. Chandrasekar, and Y. Wang, "X-band polarimetric radar network in the Tokyo metropolitan area X-NET," *Proceeding of the 5th European Conference on Radar in Meteorology and Hydrology*, July 2008.
3. Mudukutore, A. S., V. Chandrasekar, and R. J. Keeler, "Pulse compression for weather radars," *IEEE Trans. on Geoscience and Remote Sensing*, Vol. 36, 125–142, January 1998.
4. Puhakka, T., V. Chandrasekar, and P. Puhakka, "Evaluation of FM pulse compression for weather radars," *AMS 33rd Conference on Radar Meteorology*, 7.6, August 2007.

5. Mega, T., K. Monden, T. Ushio, K. Okamoto, Z. Kawasaki, and T. Morimoto, "A low-power high-resolution broad-band radar using a pulse compression technique for meteorological application," *IEEE Geoscience and Remote Sensing Letters*, Vol. 4, No. 3, July 2007.
6. Nakagawa, K., H. Hanado, K. Fukutan, and T. Iguchi, "Development of a C-band pulse compression weather radar," *AMS 32nd Conference on Radar Meteorology*, P12R.11, October 2005.
7. O'Hora, F. and J. Bech, "Improving weather radar observations using pulse-compression techniques," *Meteorological Applications*, Vol. 14, 389–401, 2007.
8. Cho, Y. G., "A high bandwidth radar operation over the internet: Signal analysis, network protocols and experimental validation," Ph.D. Thesis, Colorado State University, Fort Collins, Colorado, 2004.
9. Brotzge, J., K. Brewster, V. Chandrasekar, B. Philips, S. Hill, K. Hondl, B. Johnson, E. Lyons, D. McLaughlin, and D. Westbrook, "CASA IP1: Network operations and initial data," *AMS 23rd Conference on IIPS*, 8A.6, January 2007.
10. Junyent, F. and V. Chandrasekar, "Radar network characterization," *IEEE Geoscience and Remote Sensing Symposium, IGARSS 2007*, 2730–2733, July 2007.
11. Donovan, B. C., D. J. McLaughlin, M. Zink, and J. Kurose, "Simulation of minimal infrastructure short-range radar networks," *IGARSS 2007*, 2734–2737, July 2007.
12. Donovan, B. C., D. J. McLaughlin, M. Zink, and J. Kurose, "OTGsim: Simulation of an off-the-grid radar network with high sensing energy cost," *5th Annual IEEE Communications Society Conference on Sensor, Mesh and Ad Hoc Communications and Networks*, 506–514, June 2008.
13. Smith, C. and C. Gervelis, *Wireless Network Performance Handbook*, 4.12 Frequency Planning, McGraw-Hill, 2003.
14. Macario, R. C. V., *Modern Personal Radio Systems*, 5 Cellular Radio Planning Methods, IEE Telecommunication Series 33, 1996.
15. McLaughlin, D. J., V. Chandrasekar, K. Droege-meier, S. Frasier, J. Kurose, F. Junyent, B. Philips, S. Cruz-Pol, and J. Colom, "Distributed collaborative adaptive sensing (DCAS) for improved detection, understanding, and predicting of atmospheric hazards," *AMS 9th Symposium on Integrated Observing and Assimilation Systems for the Atmosphere, Oceans and Land Surface*, P11.3, January 2005.

16. Park, J. G., "Design and performance analysis of nonlinear FM waveform for meteorological radar," Master's Thesis, Gwangju Institute of Science and Technology, 2009.
17. Witte, E. D. and H. D. Griffiths, "Improved ultra-low range sidelobe pulse compression waveform design," *IET Electronics Letters*, Vol. 40, 1448–1450, October 2004.
18. Johnston, J. A. and A. C. Fairhead, "Waveform design and doppler sensitivity analysis for nonlinear FM chirp pulsed," *IEE Communications, Radar and Signal Processing*, Vol. 133, 163–175, April 1986.
19. Puhakka, T., P. Puhakka, and F. O'Hora, "On the performance of NLFM pulse compression with polarimetric doppler radar," *Proceedings of the 4th European Radar Conference*, 88–91, September 2006.
20. Kollias, P., E. E. Clothiaux, M. A. Miller, B. A. Albrecht, G. L. Stephens, and T. P. Ackerman, "Millimeter-wavelength radars: New frontier in atmospheric cloud and precipitation research," *Bulletin of the American Meteorological Society*, Vol. 88, 1608–1624, October 2007.
21. Krofli, R. A. and R. D. Kelly, "Meteorological research applications of MM-wave radar," *Meteorology and Atmospheric Physics*, Vol. 59, 105–121, March 1996.
22. Lee, H., S. G. Park, J. W. Jung, and Y. H. Kim, "Ka-band solid-state pulse compression for meteorological observation," *Global Symposium on Millimeter Waves*, Korea, 2010.
23. Zrnica, B. M., A. J. Zejak, and I. S. Simic, "The eclipsing zone problem in the chirp radar," *EUROCON, Trends in Communications, International Conference*, Vol. 2, 329–332, July 2001.
24. Majurec, N., "Advanced multi-frequency radar: Design, preliminary measurements and particle size distribution retrieval," Ph.D. Thesis, University of Massachusetts Amherst, 2008.
25. Lee, H. and Y. H. Kim, "A 35 GHz narrow beam lens antenna for aircraft mounting collision warning radar," *MM-wave Radar & Radiometer Forum*, Korea, 2004.